



A natural cement analogue study to understand the long-term behaviour of cements in nuclear waste repositories: Maqarin (Jordan)



Lukas H.J. Martin ^{a, b, *}, Andreas Leemann ^{a, **}, Antoni E. Milodowski ^c, Urs K. Mäder ^d, Beat Münch ^a, Niels Giroud ^e

^a Empa, Swiss Federal Laboratories for Materials Testing and Research, Laboratory for Concrete and Construction Chemistry, Dübendorf, Switzerland

^b ETH Zürich, Department of Earth Sciences, Institute for Geochemistry and Petrology, Zürich, Switzerland

^c British Geological Survey, Keyworth, Nottingham, United Kingdom

^d Institute of Geology, University of Bern, Bern, Switzerland

^e Nagra, Nationale Genossenschaft für die Lagerung radioaktiver Abfälle, Wettingen, Switzerland

ARTICLE INFO

Article history:

Received 23 December 2015

Received in revised form

17 May 2016

Accepted 18 May 2016

Available online 20 May 2016

Keywords:

Natural analogue

Nuclear waste repository

Maqarin

Cement

Porosity

Hyperalkaline plume

Reactive transport model

ABSTRACT

The geological storage of nuclear waste includes multibarrier engineered systems where a large amount of cement-based material is used. Predicting the long term behaviour of cement is approached by reactive transport modelling, where some of the boundary conditions can be defined through studying natural cement analogues (e.g. at the Maqarin natural analogue site). At Maqarin, pyrometamorphism of clay biomicrites and siliceous chalks, caused by the in-situ combustion of organic matter, produced various clinker minerals. The interaction of infiltrating groundwater with these clinker phases resulted in a portlandite-buffered hyperalkaline leachate plume, which migrated into the adjacent biomicrite host rock, resulting in the precipitation of hydrated cement minerals.

In this study, rock samples with different degrees of interaction with the hyperalkaline plume were investigated by various methods (mostly SEM-EDS). The observations have identified a paragenetic sequence of hydrous cement minerals, and reveal how the fractures and porosity in the biomicrite have become sequentially filled. In the alkaline disturbed zone, C-A-S-H (an unstoichiometric gel of Ca, Al, Si and OH) is observed to fill the pores of the biomicrite wallrock, as a consequence of reaction with a high pH Ca-rich fluid circulating in fractures. Porosity profiles indicate that in some cases the pores of the rock adjacent to the fractures became tightly sealed, whereas in the veins some porosity is preserved. Later pulses of sulphate-rich groundwater precipitated ettringite and occasionally thaumasite in the veins, whereas downstream in the lower pH distal regions of the hyperalkaline plume, zeolite was precipitated.

Comparing our observations with the reactive transport modelling results reveals two major discrepancies: firstly, the models predict that ettringite is precipitated before C-A-S-H, whereas the C-A-S-H is observed as the earlier phase in Maqarin; and, secondly, the models predict that ettringite acts as the principal pore-filling phase in contrast to the C-A-S-H observed in the natural system. These discrepancies are related to the fact that our data were not available at the time the modelling studies were performed. However, all models succeeded in reproducing the porosity reduction observed at the fracture–rock interface in the natural analogue system.

© 2016 Elsevier Ltd. All rights reserved.

1. Introduction

The accumulating nuclear waste from power plants, medical

and research facilities must be stored safely for 10^5 – 10^6 years until the radioactivity has decayed to a level below which any release of radionuclides to the environment no longer poses an unacceptable risk. In several concepts for nuclear waste storage, the galleries in which the waste containers are emplaced will be back-filled and sealed with cementitious mortars, as the highly alkaline cement pore waters are expected to limit the solubility and mobility of radionuclides, and they also provide favourable conditions for the

* Corresponding author.

** Corresponding author.

E-mail addresses: Lukas.martin@erdw.ethz.ch (L.H.J. Martin), Andreas.leemann@empa.ch (A. Leemann).

long-term stability and inhibit corrosion of the steel waste containers (www.nagra.ch, 2013: Entsorgungsprogramm und Standortgebiete für geologische Tiefenlager). Therefore, there is a need to understand the interaction of a high pH pore water plume migrating from the cement into the host rock in order to assess its impact on porosity, permeability and groundwater flow, and consequently the radionuclide transport.

Long-term predictions for the interaction of a hyperalkaline plume in contact with the host rock in a nuclear waste repository are approached by reactive transport models. However, in order to have an accuracy control for such models, they should be compared with processes occurring in natural analogue systems such as the Maqarin cement analogue site, where the interaction between a host rock and a hyperalkaline plume occurred over >100,000 years (Linklater, 1998; Smellie, 1998; Pitty and Alexander, 2014). Thus studying natural analogue systems provides the potential to understand the processes which could occur along a fracture system in a nuclear waste repository and increase the confidence in the extrapolation of data to greater time and distance scales, as indicated by Savage (2011).

Within the framework of the Long-Term Cement Study (LCS) project, data from various reports that investigated the Maqarin cement analogue site (Jordan) were compiled in order to understand the geochemical long-term processes occurring in this natural cement analogue system (Jordan Natural Analogue Project Phase I to IV: Alexander, 1992; Linklater, 1998; Smellie, 1998; Pitty and Alexander, 2014). To extrapolate the long-term effects, various studies modelled the interaction of a hyperalkaline plume along a single fracture system similar to that at the Maqarin site, in order to predict which processes occur along a fracture (e.g. Steefel and Lichtner, 1998; Shao et al., 2013; Soler, 2016; Watson et al., 2016). Within the scope of this work, the existing database on Maqarin has been extended by studying additional mineral alteration samples from Adit A6. This tunnel was constructed for the Jordan–Syria unity dam project in 1979 (Alexander, 1992; Milodowski, 1994a, b, c, d, 1998, 2013; Linklater, 1998; Smellie, 1998) and is located about 60 m above the Yarmouk river and has been driven southward along N358° for 450 m horizontally into the hill side (for details see Steefel and Lichtner, 1998). The aim of this study was to develop a conceptual model of the processes that influenced the mineralogical and geochemical evolution along the fracture flow system in Adit A6 (i.e. the mineral precipitation sequence, interaction of the hyperalkaline plume with the host rock and its impact on porosity), and further to compare the observations from the natural samples with modelling results.

A summary of the site and the hydrology are provided by Steefel and Lichtner (1998). Here we would like to highlight the key points which are important for understanding the processes which occurred along the fracture systems in Adit A6. The stratigraphy of the site is described by Houry et al. (1998) and a detailed description of these rocks is provided by Alexander (1992) and Milodowski et al. (1994a, b, 1998). The pyrometamorphic rocks that represent the cement analogue are located in the upper part of the Bituminous Marl Formation and the base of the Chalky Limestone Formation (Upper Cretaceous). The background host rocks are classified as bituminous clay-biomicroites (Folk, 1959; Pettijohn, 1975) with up to 20% organic matter (immature kerogen, Smellie, 1998). In-situ combustion of organic matter within the clay biomicroite resulted in thermal metamorphism (pyrometamorphism) which calcined the limestone and produced various minerals analogous to cement clinker phases (Alexander, 1992; Milodowski, 1994a; b, 2013). Infiltrating groundwater interacting with these “clinker” phases produced a portlandite-buffered hyperalkaline leachate plume that emanates from the “cement zone”, and leads to the formation of hydrated cement phases such as ettringite

($\text{Ca}_6\text{Al}_2(\text{SO}_4)_3(\text{OH})_{12}\cdot 26(\text{H}_2\text{O})$), thaumasite ($\text{Ca}_3\text{Si}(\text{CO}_3)(\text{SO}_4)(\text{OH})_6\cdot 12(\text{H}_2\text{O})$), tobermorite ($\text{Ca}_5\text{Si}_6\text{O}_{16}(\text{OH})_2\cdot 2-8(\text{H}_2\text{O})$), afwillite ($\text{Ca}_3(\text{SiO}_3\text{OH})_2\cdot 2\text{H}_2\text{O}$), jennite ($\text{Ca}_9\text{H}_2\text{Si}_6\text{O}_{18}(\text{OH})_8\cdot 6\text{H}_2\text{O}$), and unstoichiometric calcium-aluminium-silicate-hydrates (C-A-S-H), and amorphous calcium-aluminium-silicate-hydrate (C-A-S-H) gels.

For details about the hydrogeological setting and water geochemistry of the Maqarin site within the context of the regional flow system of northern Jordan, see Waber et al. (1998). Two distinct hyperalkaline groundwater systems have been recognized at Maqarin, referred to as the Eastern Springs and the Western Springs, respectively. Adit A6 is located within the Eastern Springs area. Both systems are Ca-OH-dominated groundwaters. However, the Western Springs groundwater are more mineralized and contain a high concentration of Na and K in addition to a higher concentration of $\text{Ca}(\text{OH})_2$, which results in a pH up to 13 in comparison to about 12.5 for the Eastern Springs area. The difference in composition of the groundwaters between the Eastern and Western springs can be explained by a difference in the extent and duration of water–rock interaction (Waber et al., 1998). The Eastern Springs groundwater is considered to be more evolved, as having more extensively leached away the more soluble and K-Na-rich metamorphic silicates that are the earliest minerals to hydrate and dissolve in the pyrometamorphic rocks (Milodowski et al., 2013). This has resulted in the Eastern Springs now having a lower pH. Therefore, the question arises whether the Western Springs represent an analogue of the “early” hyperalkaline cement pore fluid with NaOH-KOH- $\text{Ca}(\text{OH})_2$ -dominated leachate of pH up to 13 that is still in the process of leaching the very soluble K-Na-rich phases, whereas the Eastern Springs (exemplified by the groundwater discharging into Adit A6) correspond to a more evolved “later” $\text{Ca}(\text{OH})_2$ -buffered cement pore fluid with low NaOH and KOH, and a pH around 12.5 (Smellie et al., 2013). Based on stable isotope and ^{14}C analyses, it is assumed that temperatures were near ambient at the time when hydration, recarbonation and sulphatation occurred (Clark et al., 1993).

Average saturation indices for the high pH groundwater for the Western Springs area, which corresponds to the early water chemistry of the hydration of the natural clinker in Adit A6, suggest that the early Maqarin groundwater is strongly undersaturated with silicon, and will consequently tend to dissolve silicate and aluminosilicate phases (Waber et al., 1998). Furthermore, the undersaturation of CO_2 with the atmosphere explains the abundant tufa precipitates on the fracture walls in Adit A6 and at spring discharge points. With regard to this CO_2 undersaturation, carbonation could be an issue for the preservation of the hydrated cement phases. The principal seepages of hyperalkaline groundwater into the Adit A6 occur in a wide, highly brecciated fracture zone in the pyrometamorphic rocks that is intersected by the tunnel between 110 and 305 m from the entrance (Fig. 1S, Supporting Material). The abundant fractures between 110 and 140 m, which are now largely sealed by secondary calcite, C-A-S-H, ettringite and thaumasite, indicate that the extent of hyperalkaline groundwater flow in these fractures was originally much wider (Milodowski et al., 1994b). Further towards the back of the tunnel (318–370 m) there are several small fracture-controlled groundwater inflows. All major groundwater inflow zones in Adit A6 are fracture-controlled and occur within the highly brecciated, high-temperature pyrometamorphic zones intersected by the tunnel (Milodowski et al., 1994b, 2013). At around 110 m, the bituminous clay biomicroites appear to be very extensively altered and very friable. In this region, the clay biomicroite is cut by abundant, closely-spaced, fine anastomosing networks of white veinlets containing cross-fibrous to fine-powdery ettringite–thaumasite, and occasionally veins of grey white calcite (Milodowski et al.,

1994b, 1998; 2013).

With regard to the paragenesis of cement minerals evolving in the fractures, it should be noted that the “clinker”, which was part of the pyrometamorphosed rock before alteration, differs from standard Ordinary Portland Cement (OPC). It has a much lower Si + Al: Ca ratio than OPC, and no alite is present, although larnite (belite) occurs. Milodowski et al. (1994d, 2013) subdivided the sequence of alteration of the bituminous biomicrite by hyperalkaline groundwater into the following four stages referring to the high pH inflow region of tunnel A6:

- i. An aragonite-mineralisation stage resulting from the early fracture opening and initiation of hyperalkaline groundwater movement. The precipitation of aragonite on fracture walls is possibly a result of mixing of $\text{Ca}(\text{OH})_2$ -saturated groundwater with background bicarbonate waters originally present in clay biomicrite.
- ii. An ettringite–thaumasite-dominated stage, which consists of fracture-filling thaumasite (with minor ettringite in solid solution) and gypsum. Wallrock alteration was most probably initiated during this stage with the dissolution of clay minerals and calcite.
- iii. A C-S-H stage following fracture reactivation, dissolution and replacement of earlier-formed thaumasite accompanied by the precipitation of C-A-S-H or tobermorite. Major wallrock alteration occurred during this stage.
- iv. A zeolite stage resulted from the replacement of earlier C-S-H and thaumasite by fracture-sealing zeolites: initially high Si-rich zeolites of mordenite-dachiardite composition; then subsequently, zeolites progressively varying from “epistilbite” to “yugawaralite” and finally “laumontite”-like compositions, accompanied by a minor amount of gypsum. This may reflect the progressive loss of silica from the system as hyperalkaline leaching continued. It would appear that zeolite alteration has affected the wallrock only very slightly.

It should be noted that the geology of the Maqarin site is complex, with lithological variations, sometimes on cm-scale. This makes data interpretation and establishing a comprehensive picture of rock–water interaction and mineral alteration very difficult. The Adit A6 itself, and additionally the limited sample suite collected from the tunnel, may not be perfectly representative of the entire Maqarin site, but allow enough insight to establish an overall picture of the rock–water interaction behaviour, and provide a valuable opportunity to investigate the long-term effects of a hyperalkaline plume.

Within the scope of this study, various rock samples from Adit A6 were studied with the aim of developing a conceptual model of the processes that resulted in the formation of the Maqarin cement analogue. The main aspect was to understand the sequence of mineral formation of the cementitious hydrates, and the processes leading to the sealing of fractures at a large temporal and spatial scale. In particular, we discuss how the porosity of the adjacent host rock was affected by the hyperalkaline plume. Further, we compare our observations with the results from various reactive transport models from the Maqarin analogue site in order to provide inputs to the modellers on the extent to which their results coincide with our observations.

2. Sample localities and methods

2.1. Sample localities

Within the scope of the LCS Project, 11 samples from Adit A6 were investigated, and the detailed results are provided in Martin

and Leeman (2014, under review). However, in this paper, we highlight only the most important findings with regard to the evolution of the Maqarin analogue.

Images of the investigated samples are presented in Fig. 1 with locations referenced to the distance from the entrance of Adit A6. The metamorphic zone from which the hyperalkaline plume emanated occurs beyond 110–113 m from the entrance. With increasing distance from the metamorphic zone, the general degree of alteration of the samples is expected to decrease (i.e. towards the entrance of Adit A6).

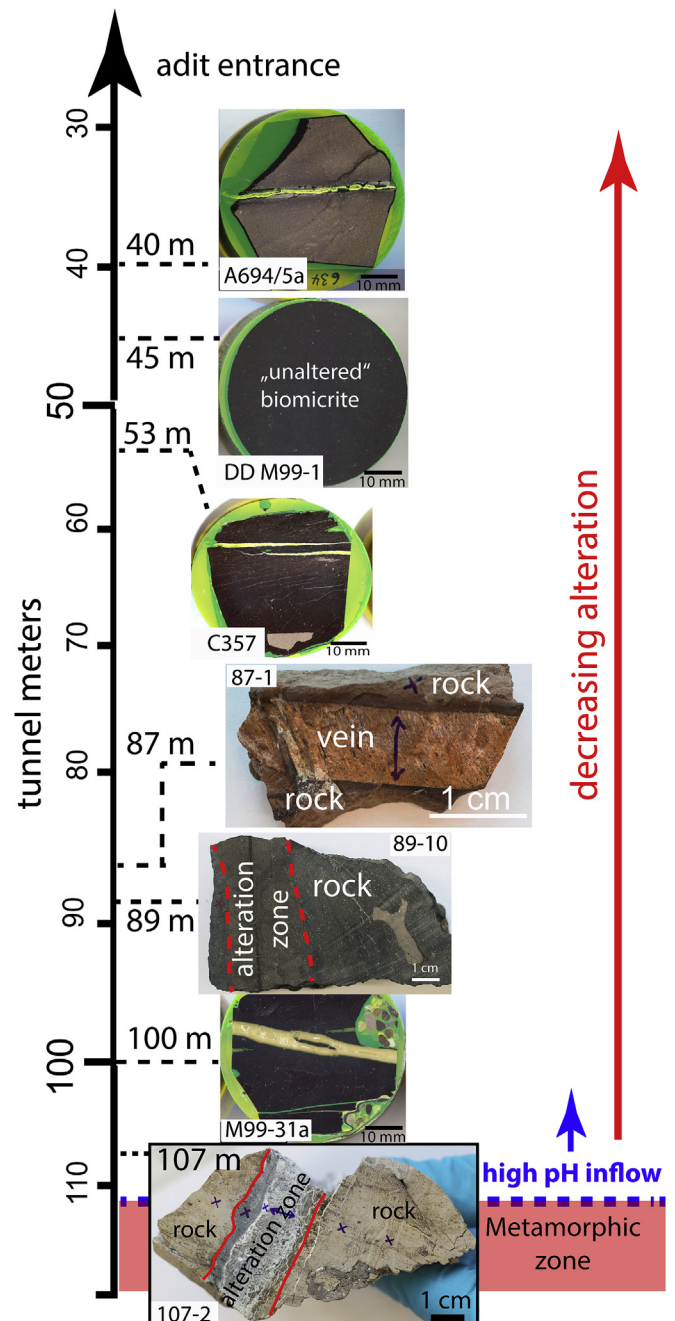


Fig. 1. Schematic cross-section through Adit A6 with sample localities and photographs of the investigated samples.

2.2. Methods

At selected points across the samples, material was removed with a microdriller for analysis by X-ray diffraction (XRD), employing a PANalytical X'Pert Pro MPD diffractometer in a Θ - 2Θ configuration, using either $\text{CuK}\alpha$ radiation ($\lambda = 1.54 \text{ \AA}$) or Co-radiation ($\lambda_{\text{K}\alpha 1} = 1.789 \text{ \AA}$, $\lambda_{\text{K}\alpha 2} = 1.793 \text{ \AA}$). The powdered samples were dispersed in acetone and deposited onto a silicon wafer, and scanned at 5 – $70^\circ 2\Theta$ with the X'Celerator detector over a period of 120 min when using Cu-radiation and for 45 min when using Co-radiation. XRD patterns were recorded using an incident beam monochromator, with a 0.5° divergent slit, a 1° anti-scattering slit, and a 0.04 rad Soller slit on the diffraction beam side.

Samples were also prepared as polished sections after impregnation with epoxy resin. These were carbon-coated and studied with a scanning electron microscope (SEM FEG XL 30, Philips) at the Swiss Federal Laboratories for Materials Testing and Research, fitted with an EDAX 194 UTW detector, a Philips digital controller, and using Genesis Spectrum Software (Version 4.6.1) with ZAF correction. A beam-accelerating voltage of 15 kV was used for imaging, or 12 kV for energy-dispersive analysis (EDS) at high vacuum conditions.

Measured phase compositions were plotted as molar ratios using ternary phase diagrams. Abbreviations used in the ternary phase diagrams are: Cc = calcite, C-A-S-H = non-stoichiometric cementitious gel phase consisting of Ca, Al, Si and OH^- , ett = ettringite, th = thaumasite, zeol = zeolite.

EDS profiles spanning a length of several millimeters based on area scans of the entire SEM image fields were performed. The analysed elements were determined as wt%. Element compositions in the profiles were normalized to a carbon-free basis. Variations in C concentrations measured by EDS area measurements, or displayed in EDS element maps, are therefore a proxy for the variation of porosity within the sample. For better phase visualization, one series of element maps from sample 107–2 were clustered using the approach of Münch et al. (2015).

The porosity of various samples was also determined by mercury intrusion porosimetry (MIP), employing a two-fold intrusion cycle, according to the procedure explained in Kaufmann et al. (2009) and Kaufmann (2010).

Water adsorption at atmospheric pressure was measured according to EN 13,755: 2008 "Natural stone method" to determine the capillary pore volume. The water vapour diffusion resistance factor was measured according to ISO-norm 12,572 (2001–06) (temperature of 23°C , relative humidity of 50%) as a parameter characterizing transport properties.

3. Results

3.1. "Unaltered" biomicrite sample (DD-M99-1)

Sample DD-M99-1 is a core taken from the M2 seepage zone 45 m from the tunnel entrance (Fig. 1 and 1S (Supporting Material)). The investigated sample was taken from the end of the 360 cm long core drilled into the adit wall, and consists of "unaltered" biomicrite. As such, it represents the end-member background host rock at Maqarin in regard to having the "least" alteration.

Qualitative XRD results indicate that the sample consists mostly of calcite and significant amounts of hydroxylapatite. Quartz, kaolinite and gypsum have been determined as minor phases and afwillite/illite, magnetite and zeolite occur as traces.

The high calcite concentration is also reflected by the high CaO and inorganic carbon content (Table 1). Additionally, the sample contains 10 wt% organic carbon. Modal mineral contents have been

Table 1
XRF composition and calculated modal mineral contents [wt%].

	XRF	Calculated modal mineral contents	
	DD M99-1		DD M99-1
SiO_2	4.25	Calcite ^a	59.8
TiO_2	0.07	Apatite ^b	6.2
Al_2O_3	1.65	Dolomite ^c	1.07
Fe_2O_3	0.69	Kaolinite ^d	8.4
Cr_2O_3	0.04	Quartz ^e	3.0
MnO	0.01	C^{org}	10.0
MgO	0.23	Pyrite ^f	0.1
CaO	44.24	Gypsum ^g	8.4
Na_2O	0.12	Unknown minerals	3.0
K_2O	0.33	Total	100.0
P_2O_5	1.75		
SO_3	4.43		
L.O.I.	41.89		
Total	99.69		
C^{Total}	17.18		
TOC	9.97		
C^{anorg}	7.21		

^a Calcite calculated from C^{anorg} remaining after dolomite calculation.

^b Apatite calculated from P_2O_5 .

^c Maximal dolomite content calculated from MgO.

^d Maximal kaolinite content calculated from Al_2O_3 .

^e Quartz is estimated to correspond to 70% of the SiO_2 content.

^f Maximal pyrite content calculated from Fe_2O_3 .

^g Maximal gypsum content calculated from SO_3 remaining after pyrite.

calculated for dolomite (accounting for MgO), calcite (accounting for the remaining inorganic carbon), apatite (accounting for the P_2O_5), kaolinite (from Al_2O_3) and attributing the remaining 70% of the SiO_2 to quartz. Maximum pyrite content was calculated based on Fe_2O_3 and maximum gypsum content accounting for the remaining SO_3 . It should be noted that these are maximal estimates, as part of the inorganic carbon, phosphate, aluminium and SiO_2 can also be incorporated into other phases. Although there are uncertainties related to these calculations, the results provide a reasonable estimation of the modal mineral contents although the amount of gypsum is probably overestimated since some of the sulphur may be present as organic sulphur.

The biomicrite consists of fragments of calcareous foraminifers (Fig. 2S–A, Supporting Material). A few of the foraminifers are filled with iron sulfides, as indicated by the EDS analyses. The BSE image in Fig. 2S–B (Supporting Material) shows fragmented foraminifers and other bioclasts consisting of calcite. They are cemented by an interstitial medium grey gel. In addition, apatite has been found in this sample. Fig. 2S–C (Supporting Material) shows an elongated detrital grain of illitic composition within a biomicrite matrix composed mostly of calcite. The interstitial grey gel (seen in the lower left corner of the BSE image in Fig. 2S–C, Supporting Material) shows a trend towards zeolitic composition corresponding to approximately $\text{KCa}_5\text{Si}_4\text{Al}_2\text{O}_{17} \cdot x\text{H}_2\text{O}$. It should be noted that neither C-A-S-H, C-S-H, ettringite nor thaumasite were identified by XRD nor SEM-EDS analysis in the sample. Overall, petrographic examination shows very limited formation of C-A-S-H gel, which indicates that this sample has been affected by the hyperalkaline plume to only a small degree. The presence of the zeolite gel may indicate only very weak alteration of the biomicrite.

The biomicrite (Fig. 3S, Supporting Material) displays a pore size distribution mainly in the range of 10–110 nm, amounting to a total porosity of 33.6 vol%.

Results for water adsorption show a porosity accessible by capillary suction of 32.7 vol%. A water vapour diffusion resistance factor characterized by a μ -value of 23.8 was determined. For comparison, air per definition has a μ -value of 1 and a dense natural limestone or marble a μ -value of 20–40, a sandstone >20 (Weber,

1983), and an almost impermeable polymer sheet a μ -value of 10,000 according to DIN EN 12572. These results show that the unaltered biomicrite from Maqarin Adit A6 has a high porosity but a relatively high water vapour diffusion resistance, indicative of finely divided but connected pores and probably a relatively large capillarity. Based on the morphological evidence, the hyperalkaline plume emanating from the clinker body mainly progressed along fractures. Excluding fractures, mass transport from the hyperalkaline plume into the biomicrite would depend on its water saturation state. In the case of a saturated biomicrite, transport would be governed by diffusion or subordinate advection. In an unsaturated biomicrite, capillary suction would enable considerably faster initial pore water transport. However, the observed interaction of the hyperalkaline fluid with the biomicrite along fractures suggests that diffusion was the main transport mechanism (as will be shown later).

3.2. Sample 107-2

Sample 107–2 was collected from 107 m distance along the tunnel (Fig. 1) and is within the main alteration zone, which had the strongest interaction with the hyperalkaline plume. The rock mostly consists of calcite and hydroxylapatite. The alteration zone contains a few narrow 20–80 μm wide microfractures lined with calcite.

Fig. 2 shows typical fracture mineralisation occurring in sample 107–2. The EDS element maps indicate that the rock matrix is gradually enriched in Si and Al with decreasing distance from the microfracture walls (i.e. to the right in Fig. 2C and D). This enrichment of Si and Al results from the infiltration of the rock by a fluid precipitating C-A-S-H. As a consequence, the matrix porosity in the sample is reduced, as indicated by the decreased concentration of C (i.e. representing the epoxy-resin-filled pores) in this part of the sample (Fig. 2F). At a later stage, dilating fractures were filled with ettringite (Fig. 2E) precipitated from a later Ca-Al-S-rich fluid as the groundwater system evolved. This later fluid did not penetrate into the biomicrite, because the matrix porosity was substantially reduced after the C-A-S-H precipitation.

Further into the more altered and highly fractured part of this sample, the fracture mineralisation and wallrock alteration changes

(Fig. 3A and B): The element maps (Fig. 3C & D) indicate that, again, Si and Al are enriched within the previously porous biomicrite but sulphate concentration is lower within these zones (Fig. 3E). The porosity in the wallrock is still relatively high compared to the adjacent fracture fill and it includes “patched” zones. This indicates that within the wallrock, the matrix porosity was not completely sealed by secondary phases. In a later stage, a crack within the fracture fill opened and was subsequently mineralized by ettringite. This shows that a Ca-Al-sulphate-rich fluid was circulating through the fracture system during this stage. EDS analyses show that the “patched” inclusions within the ettringite fracture fill contain both Si and S but no Al, indicating that this phase is thaumasite ($\text{Ca}_3\text{Si}(\text{CO}_3)(\text{SO}_4)(\text{OH})_6 \cdot 12(\text{H}_2\text{O})$).

The history of the phase evolution can be visualized by the clustered EDS element maps (Fig. 3G). In a first stage, C-A-S-H-rich fluid impregnated the rock without filling the matrix porosity completely as in Fig. 2. In a later stage, a more sulphate-rich fluid resulted in the precipitation of ettringite within the fractures. In the part that was already enriched with Si, thaumasite formed instead of ettringite, filling the pores. An important point from these observations is that thaumasite only appears to form from the sulphate-rich solutions, where the biomicrite has already been enriched in silica. Additionally, all available aluminium has to have been used up by ettringite formation (Schmidt et al., 2008).

3.3. Sample M99-31a

Sample M99-31a, which was taken at 100 m from the adit entrance, contains a vein which is crosscutting the biomicrite host rock (Fig. 1). XRD analyses show that the biomicrite consists mostly of calcite and hydroxylapatite. Quartz, dolomite and kaolinite occur as minor components. The vein consists largely of C-A-S-H with a rather uniform composition (Fig. 4A–C). Within the central part of the vein, irregular patches of calcite are abundant and partly replace the C-A-S-H (Fig. 4A, B). This pattern could be the result of C-A-S-H carbonation. A thin fringe of calcite lines the wall of the vein (seen in the upper part of the vein in Fig. 4D). This calcite appears to have formed by an initial precipitation of calcite before the fracture further opened and C-A-S-H precipitated. Alternatively, it could be speculated that an initial crack could have been filled

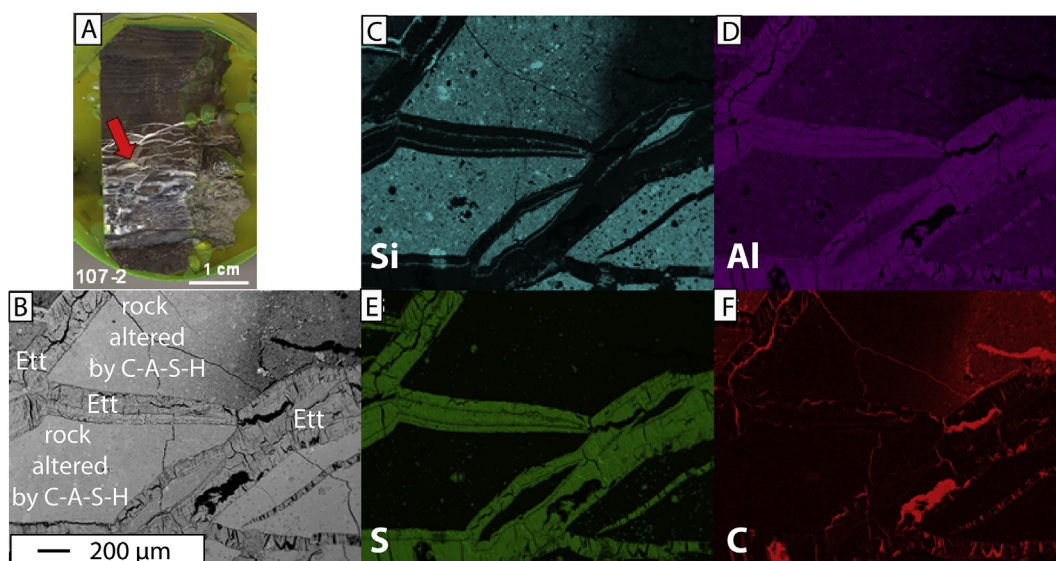


Fig. 2. A) Photograph of sample. The arrow shows the location of the BSE images. B) BSE image. C-F) EDS element maps of Si, Al, S and C. The latter showing the porosity of the sample. Abbreviation: Ett = ettringite.

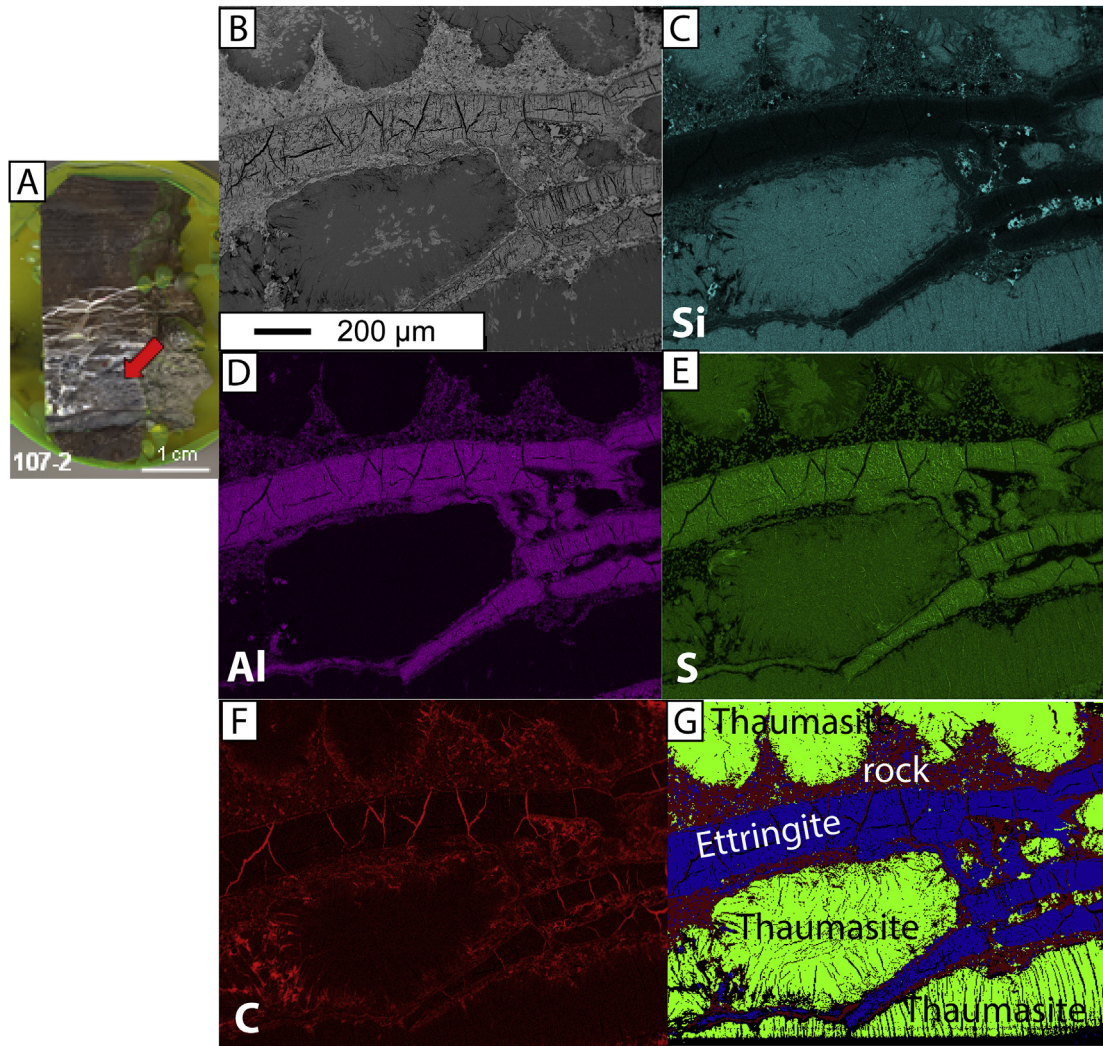


Fig. 3. A) Photograph with location. B) BSE image. C-F) EDS element maps of Si, Al, S and C, the latter showing the porosity of the sample. G) Clustered element maps.

with portlandite, which was subsequently altered to calcite as the pH dropped. The low backscatter contrast of the dark phases within the vein (Fig. 4B and D) and their high carbon signal in EDS analyses (not shown) show that a significant part of epoxy resin is present in the impregnated vein. This indicates that the vein is significantly more porous than the surrounding biomicrite. The higher BSE contrast seen in the wallrock immediately adjacent to the C-A-S-H vein (Fig. 4A) indicates that calcite precipitated within the biomicrite, thereby decreasing its porosity within a narrow band immediately adjacent to the vein.

3.4. Sample 87-1

Sample 87–1 was taken at 87 m from the entrance of Adit A6 (Fig. 1) and contains a vein consisting of calcite and C-A-S-H cutting the biomicrite host rock. Adjacent to the vein there is an alteration zone (Fig. 5), where pores are filled by C-A-S-H. The porosity of these three zones was measured by mercury intrusion porosimetry (Fig. 5). The highest porosity, up to 51%, was measured in the vein, whereas the maximum porosity in the biomicrite is 47%. The pores within the altered wallrock zone are filled by C-A-S-H and result in the lowest porosity (19%). However, the step-like shape of the MIP porosity curves for the host rock and the alteration zone indicates

that during the mercury intrusion measurements, the pore size distribution is altered, presumably by pore wall compression.

3.5. Sample 89-10

Sample 89–10 was collected 89 m from the adit entrance and comprises a 3–4 mm wide fracture alteration zone within the biomicrite (Fig. 1). Qualitative XRD analyses indicated that the biomicrite consists mostly of calcite with a small amount of kaolinite and hydroxylapatite. BSE images show that the alteration zone consists mostly of calcite and tobermorite, with irregular diffuse or “cloud-like” patches of thaumasite typically close to the sulfide-bearing parts of the wallrock (not shown here; for details see Martin and Leemann, 2014 and under review).

BSE images and corresponding EDS element maps were recorded along a profile across the alteration zone (Fig. 6A). Due to the presence of C-A-S-H and lower amounts of carbonates within the alteration zone compared to the biomicrite, there is an enrichment of Si relative to Ca (Fig. 6B). C-A-S-H is located in microfractures present in the alteration zone. The typical veins contain two types of these C-A-S-H phases as indicated in EDS analyses (Fig. 7). The pores in the altered biomicrite adjacent to these veins are also partially filled with C-A-S-H.

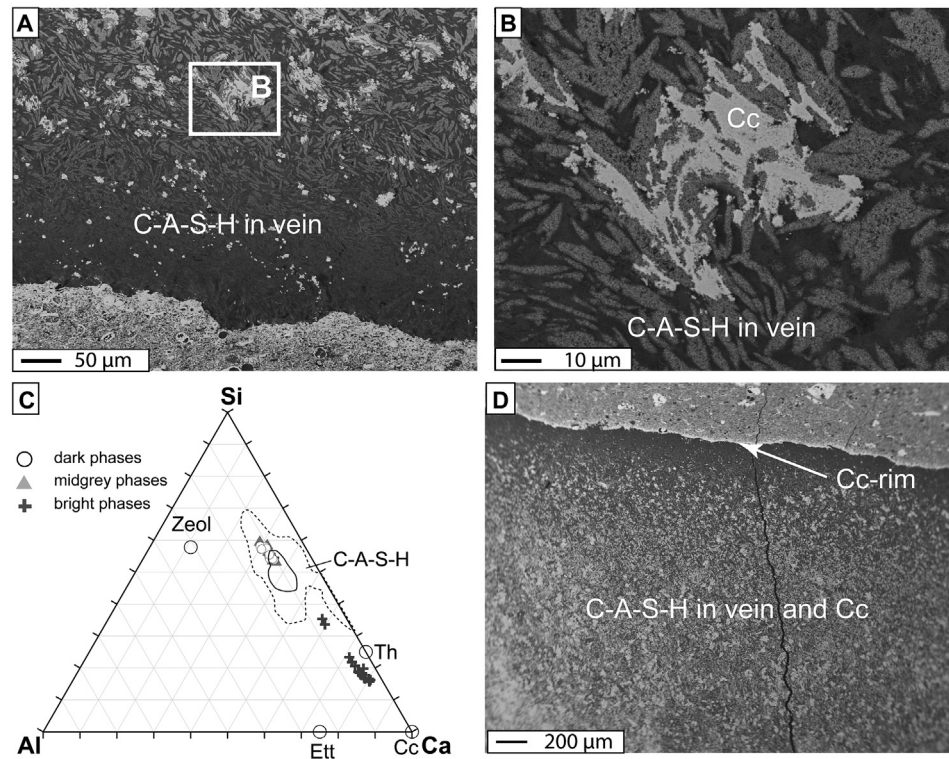


Fig. 4. A, B & D) BSE images of the vein crosscutting the biomicrite. C) EDS analyses of phases in B) plotted as at.%. The dashed range corresponds to the compositional range of observed C-A-S-H gels and the solid line ranges the recrystallized C-A-S-H phases according to AE Milodowski (unpublished report document). Abbreviations: Cc = calcite, Ett = ettringite, Zeol = zeolites.

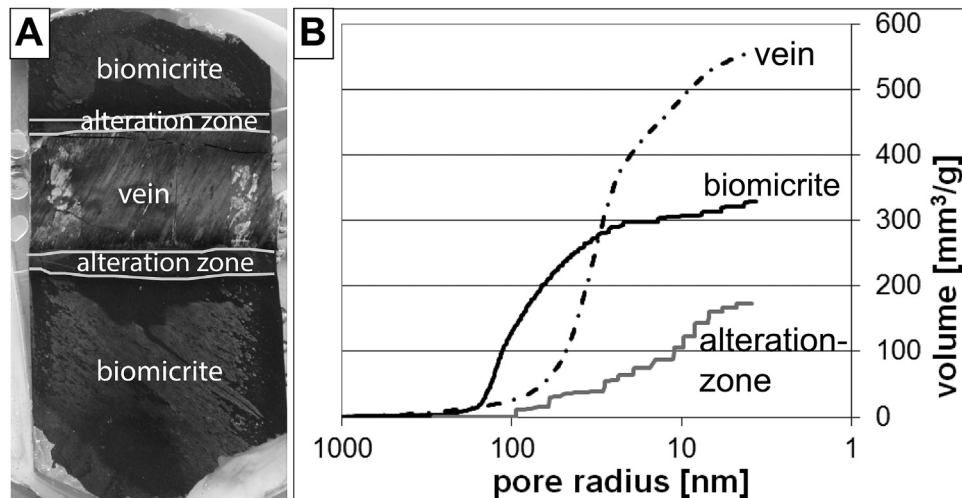


Fig. 5. A) Sample 87-1 showing the vein, alteration zone and biomicrite (for a colour image, see Fig. 1). B) Porosity measured by mercury intrusion porosimetry of the vein, the biomicrite and the alteration zone.

The precipitation of C-A-S-H in the microfractures and pores of the biomicrite reduced the overall porosity within the alteration zone (as indicated by the lower impregnation by epoxy resin and visualized by EDS mapping for carbon (for details see [Martin and Leemann, 2014 and under review](#))), in comparison to the adjacent biomicrite (Fig. 6B: note that the spikes in the carbon distribution profile correspond to cracks filled with epoxy resin).

3.6. Sample C357

This sample was taken at 53 m from the entrance of Adit A6 (Fig. 1). The biomicrite here consists mostly of calcite with minor amounts of hydroxylapatite and gypsum. The sample is cut by two large veins (Fig. 1) that contain a thin rim of C-A-S-H along the vein margins (Fig. 8C and D). The central part of the vein consists of coarse ettringite crystals. This vein filling sequence indicates that in a first stage the fractures were initially filled with C-A-S-H, and

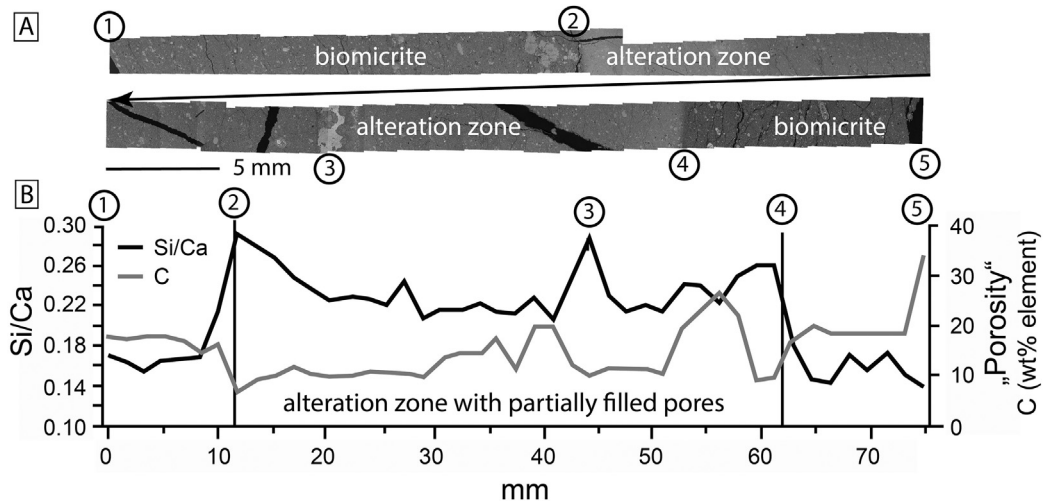


Fig. 6. A) BSE image profile taken through the rock and the alteration zone of sample 89–10. B) Ca:Si ratio measured by EDS along the profile, and C concentration from epoxy resin impregnation reflecting the variation in porosity along the profile.

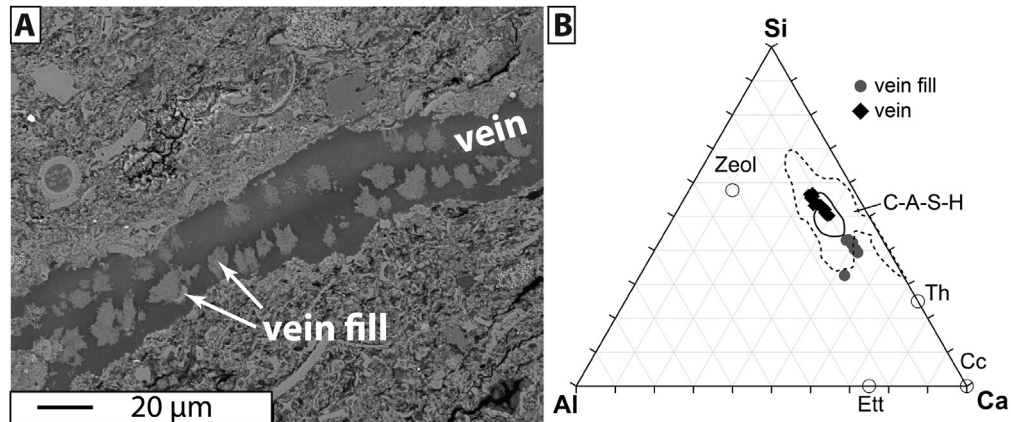


Fig. 7. A) BSE image of a vein filled with C-A-S-H occurring in the alteration zone of sample 89–10. B) Element ratio from EDS analysis: two types of C-A-S-H phases occur within the vein present in the alteration zone. For abbreviations and range of C-A-S-H composition see Fig. 4.

subsequently the fractures were reactivated and ettringite was precipitated. As indicated above, this could be explained by the average saturation indices of the high pH groundwaters from the Western Springs from Waber et al. (1998), which represents the early groundwaters that interacted with the cement clinker body. The solubility product of gibbsite in this hyperalkaline water is -4.58 , -4.05 for quartz and -4.48 for chalcedony. For gypsum it is -0.11 and calcite is oversaturated. These saturation indices suggest that only minor amounts of Si and Al could be dissolved in the early alkaline waters, similar to those from the Western Springs. Therefore these elements tend to precipitate before the sulphate phases and calcite. This would indicate that the coarse fractures were initially filled with C-A-S-H, whereas SO_4^{2-} , Ca^{2+} and CO_3^{2-} remained in the fluid. At later stages, ettringite started to precipitate when a sulphate-rich solution passed through the reopened fractures.

It is important to note that in the coarse veins, ettringite does not form a solid solution with thaumasite. However, in the smaller fractures ettringite–thaumasite solid solutions or intimately intergrown ettringite and thaumasite crystals are abundant. The smaller fractures do not show vein margins mineralised by C-A-S-H. However, the adjacent biomicrite wallrock does have an Si-Al-rich gel present, different in composition to C-A-S-H, indicating

that carbonation occurred in a late stage, as will be explained below. Furthermore, these ettringite veins do not display a wallrock alteration band in the adjacent biomicrite, in contrast to that observed for the coarser veins, suggesting that the penetration of the hyperalkaline fluids into the wallrock was only minor in veins where ettringite was precipitating.

3.7. Sample A694-5a

Sample A694-5a was taken at 40 m distance from the entrance of Adit A6 (Figs. 1 and 9). XRD results indicate that the biomicrite mostly consists of calcite and hydroxylapatite. Quartz and kaolinite were detected as minor phases by XRD, but they could not be identified by EDS analyses. However, the matrix of the biomicrite adjacent to the vein is strongly enriched in C-A-S-H (Fig. 9), which is X-ray amorphous. The zeolite is identified as chabasite on the basis of its composition determined by EDS and the XRD analyses (results from average EDS measurements on a volatile free basis in at%: Si = 31.4%, Ti = 0.5%, Al = 17.1%, Fe = 1.1%, Mg = 0.4%, Ca = 3.9%, Na = 0.5%, K = 7.6%, O = 37.1%). The zeolite may have formed at the same stage as C-A-S-H or by later alteration.

The relative porosity was assessed by EDS mapping of the C distribution along a profile perpendicular to the vein (for details,

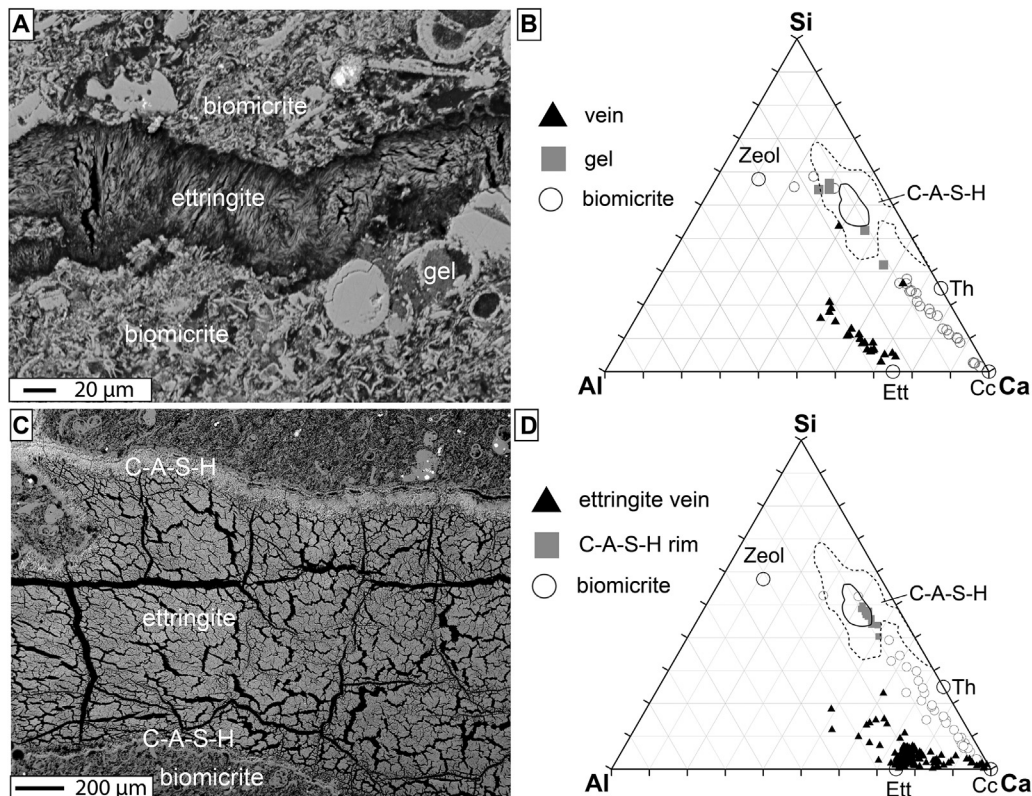


Fig. 8. A & C) BSE images. B & D) EDS analyses of phases plotted as at.%. For abbreviations and range of C-A-S-H composition see Fig. 4.

see Martin and Leemann, under review). The porosity in the biomicrite is relatively uniform but decreases in the parts of the vein filled with C-A-S-H. The areas of biomicrite where zeolites have formed display a lower porosity than the biomicrite in general or the parts of the vein filled with C-A-S-H. The limited extent of C-A-S-H formation in the biomicrite can be explained by the pore water saturation of the biomicrite limiting penetration of the wallrock by the Si-Al rich fluids from the fracture, as explained in section 4.1.

3.8. Summary table of the results

A summary of the mineral assemblage in the biomicrite, the vein mineralogy and the interaction of hyperalkaline fluid with the biomicrite is shown in Table 2.

4. Discussion

4.1. Evolutionary model of the Maqarin analogue site

Based on the existing literature and our observations, we suggest the following sequence of events at Maqarin. Initially in the Miocene, there was active faulting in the Maqarin area, which occurred with a maximal stress vector along a north–south direction (Degnan et al., 2013). Due to these stress fields, several generations of fractures were episodically opened as the Maqarin site evolved.

Groundwater infiltrating along these fractures hydrated the “natural cement clinker” (pyrometamorphic) bodies and produced a hyperalkaline leachate that migrated along the fracture systems from the pyrometamorphic bodies into the biomicrite. The fracture system at Maqarin is presumed to be highly dynamic, as earthquakes and landslips are common in the region. As a result,

fractures episodically opened and were mineralized by several generations of fluids, leading to the precipitation of a complex sequence of hydrates as the fluids evolved. Along these fracture flow paths, the fluid composition extensively evolved over distance and time. It can be assumed that multiple generations of parallel fracture systems existed, with different dimensions in their extent and periodic accessibility to the migrating hyperalkaline fluids, and still exist today. Based on the petrographic observation of the samples examined in this study, we suggest that the following sequence of mineral formation occurred (Fig. 10). It should be noted that the alteration sequence shown schematically in Fig. 10 is a simplification and represents an “idealized fracture” at the Maqarin site:

4.1.1. Portlandite/calcite precipitation

In samples 107–2, M99-31a, and C357, the veins typically display very thin rims consisting of calcite. This could be the result of an initial precipitation of portlandite, which was converted to calcite as the pH of the fluid passing through the fractures dropped. As such, this agrees with the observations from Milodowski et al. (1994d; 1998), who suggested that in the first stage portlandite precipitated and was quickly converted to calcium carbonate caused by a pH decrease and an increase in carbonate/bicarbonate in solution.

4.1.2. C-A-S-H precipitation (Fig. 10B)

In the next stage, C-A-S-H started to precipitate from the hyperalkaline fluids. Some veins occurring in samples M99-31a (from 100 m), 87–1 (87 m), consist solely of C-A-S-H with minor amounts of calcite whose origin will be discussed later. Other veins contain C-A-S-H rims on both sides of the fracture. The central parts of the veins were filled with ettringite or ettringite–thaumasite

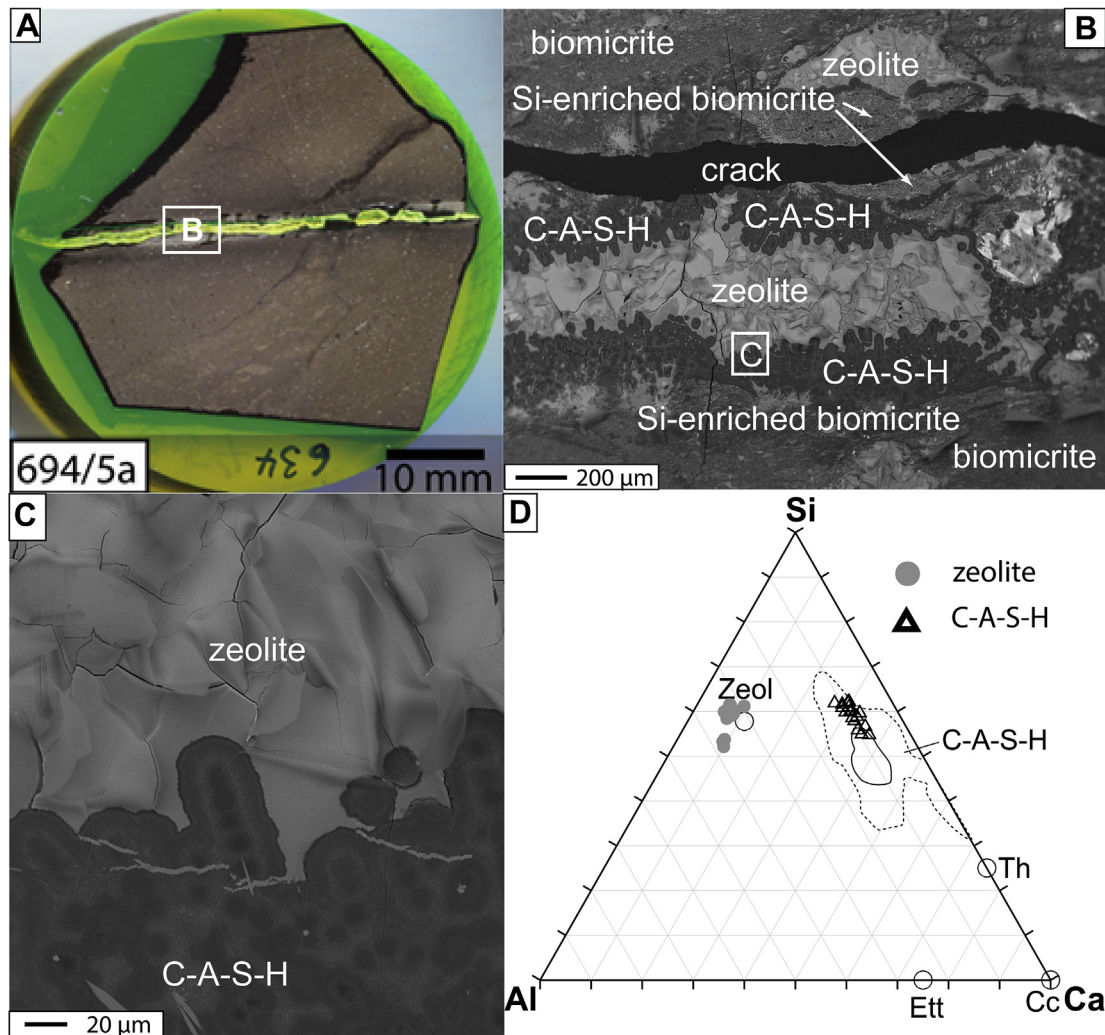


Fig. 9. BSE images of the sample with corresponding EDS analyses. For abbreviations and field for C-A-S-H composition see Fig. 4.

solid solutions, or complex intergrowths of thaumasite and ettringite (samples 107–2; C357). This indicates that in a first stage C-A-S-H initially precipitated.

4.1.3. C-A-S-H penetration into the biomicrite (Fig. 10B)

The fluid producing the C-A-S-H precipitation in the veins also impregnated the adjacent biomicrite wallrock, resulting in a reduction in porosity immediately adjacent to the veins (samples 107–2, 89–10, 87–1, C357). This process is most prominent in sample 87–1, where the porosity of the biomicrite adjacent to a 1.2 cm wide vein consisting of C-A-S-H is dramatically reduced for up to 4 mm from the vein margin (Fig. 5). However, in some samples penetration of C-A-S-H into the biomicrite has not been observed. The degree of penetration could be related to a pre-saturation of the porosity in biomicrite with background groundwater. As the pores were already water-filled, only limited diffusion of Si and Al into the pores would have occurred. Conversely, in sample 107–2, which was close to the clinker body where the combustion event occurred, due to the heating during the pyrometamorphism any pore water would probably have been expelled, leaving gas-filled pores. These open pores could therefore be more easily saturated by the Si-rich Al-bearing hyperalkaline groundwater following groundwater re-saturation and subsequent leaching of the metamorphic rocks.

4.1.4. Sulphate phase precipitation (ettringite, ettringite–thaumasite (ss) and thaumasite) (Fig. 10C)

The veins with C-A-S-H margins typically contain ettringite, ettringite–thaumasite solid solutions, or an intimate mixture of both minerals within their central parts (samples 107–2, C357). The saturation indices suggest that only minor amounts of Si and Al can be dissolved in the water (Waber et al., 1998). Therefore, these elements tend to precipitate before sulphate and calcite, which supports the observations that C-A-S-H precipitated before the sulphate phases. This would explain that the coarse fractures were initially filled with C-A-S-H, whereas SO_4^{2-} , Ca^{2+} and CO_3^{2-} remained in the fluid. In the samples, there are various generations of veins, (i) consisting solely of ettringite, (ii) forming a solid solution (ss) between ettringite and thaumasite (Barnett et al., 2002), and (iii) single patches of thaumasite. For the precipitation of ettringite, S and Al are the limiting elements. If sufficient sulphate is available, ettringite can be stabilized and if additional Si is incorporated ettringite–thaumasite solid solution are formed as observed in sample 107–2. This clearly indicates that thaumasite was formed in areas where first C-A-S-H precipitated. At a later stage, the evolution to a more S- and Al-rich fluid would lead to ettringite precipitation. However, as Al was not present in a sufficient amount to incorporate all the available sulphate in solution in ettringite, thaumasite formed instead. This sequence is sometimes

Table 2
Summary table of the biomicrite- and vein mineralogy and fluid interaction with the biomicrite.

Tunnel meters	Sample	Composition of biomicrite					Vein mineralogy					Fluid interaction with biomicrite			Comment	
		Calcite	Hydroxylapatite	Quartz	Kaolinite	Illite	Gypsum	C-A-S-H	C-A-S-H rim	Ettringite	Thaumasite	Calcite	Zeolite	Carbonation (Si-Al-gel + cc)		C-A-S-H precipitation in biomicrite reducing porosity
45	DD-M99-1	XXXX	XX	X	X	(X)	X						✓	-	-	"unaltered" biomicrite (bm) bm impregnated by C-A-S-H
107	107-2	XXX	XX				XX	XX	X				?	✓	<25	
100	M99-31a	XXXX	XX	X	X		XXX		X				✓	(-/✓)	0.3	bm impregnated by C-A-S-H
89	89-10	XXXX	XX	X	X		XXXX	X	XXX				?	✓	<25	bm impregnated by C-A-S-H
87	87-1	XXXX	XX	X	X		XXXX		X				✓	✓	<4	bm impregnated by C-A-S-H
53	C357	XXXX	XX	X	(X)		X	XX	XXX				?	(✓)	0.35	only alt. zone on top of vein
40	A694-5a	XXXX	XX	X	X		XXX					XXX	?	-	-	bm partly impregnated

XXXX = major phase, XXX = abundant major phase, XX = minor phase, X = traces, ✓ = observed, (✓) = observed at few localities.

? = unclear, - = absent

Abbreviation: bm = biomicrite

observed in concrete exposed to sulphate attack (Leemann and Loser, 2011). A decrease in pH favouring the formation of thaumasite instead of ettringite can be excluded, as both minerals occur together.

4.1.5. Zeolite precipitation in veins (Fig. 10D)

Sample A694-5a (40 m) is crosscut by a vein consisting of bands of C-A-S-H and zeolite, possibly a chabasite according to XRD and EDS analyses. Chabasite is a zeolite which forms under Si-saturated conditions (Barrer, 1977; Savage, 1998). As indicated by Savage (1998), Al and Si in cement pore fluids have a low thermodynamic activity due to the elevated pH. Therefore, these types of fluids are incapable of precipitating zeolites without a decrease in pH and reaction with a source of Si and Al. As the presence of zeolites in sample A694-5a could be clearly identified, this indicates that the pH of the pore fluid must have been reduced dramatically towards neutral pH conditions by this stage, and corresponds to the conditions prevailing at a distance from the clinker body and its emanating hyperalkaline plume.

4.1.6. Carbonation stage (Fig. 10E)

Most samples have suffered from carbonation, as was also observed by Milodowski et al. (2013). With ongoing carbonation, the primary C-A-S-H is altered to a mixture of Si-Al-rich gel and calcite (e.g. sample M99-31a). Carbonation is a common process observed in mortars and concrete exposed to atmospheric CO₂ or dissolved CO₂ or HCO₃⁻ in groundwater. Cement hydrates phases are known to readily react with CO₂ and moisture, and are transformed to CaCO₃ and a silica-rich gel containing some aluminium (Groves et al., 1991; Bary and Sellier, 2004; Leemann et al., 2015). The kinetics of natural carbonation is dependent on relative humidity, with maximum rates between 55 and 75% (Wierig, 1984). The ingress of the carbonation front into mortar and concrete slows down following a square root of time relation. After an exposure to sheltered outdoor conditions for 10 years, a concrete of the strength class C25 produced with ordinary Portland cement may display a depth of carbonation of 15–20 mm (Thomas et al., 1992). C-A-S-H is more sensitive to carbonation than ettringite and thaumasite due to its low degree of crystallinity. Patterns in C-A-S-H showing domains rich in calcium and domains poor in calcium (e.g. sample C357) indicate a carbonation of the initial phases. We suggest that some of these Si-Al-rich gels have been misinterpreted as zeolites in the past, as there is typically a trend from calcite towards the zeolite field in the ternary projections. The stage in which carbonation occurred cannot be deduced. However, Waber et al. (1998) indicated that the waters have a strong tendency to absorb CO₂ as they come into contact with the atmosphere. Additionally, the samples studied in this project have been stored in laboratories for several years and have therefore been exposed to CO₂.

4.2. Summary and discussion of the reactive transport modelling results from the Maqarin site

Various reactive transport models have been used to model the interaction of a hyperalkaline plume along an idealized fracture system at Maqarin (Steeffel and Lichtner, 1998; Shao et al., 2013; Watson et al., 2016; Soler, 2016) in order to up-scale processes that could occur in a nuclear waste repository. The focus of these studies was to evaluate the impact of water–rock interaction with the host rock along a fracture flow-path. In this section we aim to summarise the modelling results and compare how they fit with our observations from the Maqarin cement analogue site.

Steeffel and Lichtner (1998) employed a multicomponent numerical reactive transport model to simulate the flow of hyperalkaline groundwater along discrete fractures at Maqarin. They

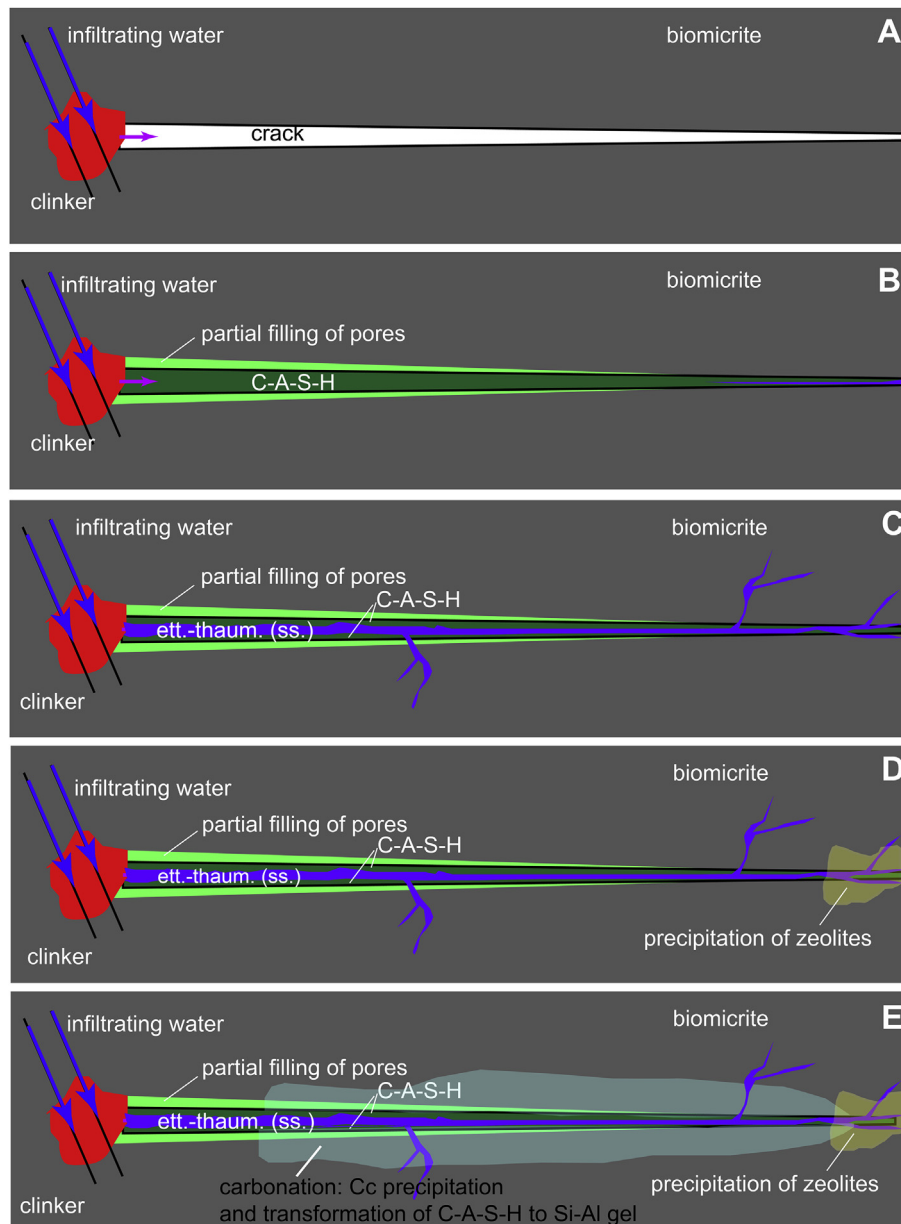


Fig. 10. Simplified cross-section along a fracture in Adit A6 along which passing fluids are evolving. A) Opening of fracture, evtl. with portlandite precipitation and conversion of the latter to calcite. B) C-A-S-H precipitation in fracture with penetration into biomicrite. C) Evolved fluid precipitates sulphate phases such as ettringite/thaumasite. D) Precipitation of zeolite at low pH in the far-field of the clinker body. E) Carbonation of C-A-S-H to Si-Al-rich gels with precipitation of calcite. Abbreviations: Cc = calcite, ett = ettringite, th = thaumasite, (ss) = solid solution.

modelled a 1-D fracture between the M1 and M2 sampling sites, along which the alteration intensity progressively decreases. Their simulations predict that ettringite, with lesser amounts of hillbrandite and tobermorite, will be the dominant alteration products, forming at the expense of the primary silicates in the rock matrix and within the fracture walls.

Shao et al. (2013) used 1-D reactive transport models to calculate the geochemical evolution of the Maqarin marl rock formation with diffuse exchange of solutes across the fracture wall. The porosity reduction processes were divided into three stages, based on the minerals involved. In the first stage, at the front of the alkaline water ingress, illite and kaolinite are dissolved, providing the Si and Al that are needed for the zeolite formation. In the second stage within 5 mm from the fracture, C-S-H phases start to precipitate in combination with ettringite, leading to a porosity

reduction over time. Ettringite becomes more important as the availability of Si and Ca becomes lower with greater distance from the fracture where straetlingite precipitates. In the third stage, continuing porosity reduction slows down the transport of chemical components and after about 500 years the maximum porosity reduction is reached at about 3 mm from the fracture (Shao et al., 2013). Based on these results, Shao et al. (2013) concluded that ettringite precipitation is the dominant phase responsible for the pore clogging, as postulated previously by Steefel and Lichtner (1998).

Soler (2016) performed 2-D calculations accounting for advection and dispersion along a single fracture system combined with diffusion into the host rock, where solute transport was coupled with mineral dissolution and precipitation. The flow-rates employed by Soler are lower than in the other studies. The

largest amounts of precipitates, responsible for porosity sealing, are predicted to form at the fracture inlet, resulting in fracture fills consisting of ettringite within the first 10 cm, with major amounts of C-S-H (with tobermorite and calcite) forming up to about 7 m downstream. This is accompanied by significant dissolution of chalcedony, kaolinite, albite and dolomite and minor amounts of muscovite along the first 10 m of the fracture flow path, providing the Si required for C-S-H and C-A-S-H mineralisation.

Watson et al. (2016) used a pseudo 2-D (1.5-D) approach to simulate the flow along the fracture and diffusion of solutes into the rock matrix. They differentiated two cases. The first case was without fracture armouring (the “base case model” according to their terminology). The second case included fracture-armouring. In the “base case model” the fracture starts to fill with ettringite together with some calcite and C-S-H in the form of jennite, resulting in almost all of the pores being filled after about 70 years. In a second stage, between 70 and 250 years, gradual dissolution of ettringite is predicted, resulting in rejuvenation of the fracture porosity. However, further sealing occurs closer to the fracture inlet after 220 years because of the precipitation of calcite and C-S-H (jennite). Further downstream, small amounts of gismondine (a zeolite) are predicted to form in response to the conversion of jennite to tobermorite. This resulted in an upstream movement of the reaction front. The dissolution of almost all the ettringite led to a downstream precipitation of thaumasite because of the release of sulphate, Si and Al ions. After 360 years, the fracture is finally filled with C-S-H, calcite and thaumasite, whereas ettringite and C-S-H phases precipitate in the wallrock close to the fracture.

In the fracture-armouring model (Watson et al., 2016), there is no ettringite, but jennite and calcite are precipitated through time along the fracture. Within the clay biomicrite, there is little difference from the base case, although there is less dissolution of primary minerals such as chalcedony due to the armouring effect. Thus, Watson et al. (2016) conclude that the latter model is more consistent with the way minerals actually precipitate although they point out that the mineralogy differs in comparison to the one observed at Maqarin.

Comparison of our observations with the model results reveals that the major discrepancy is the precipitation of ettringite before C-S-H in the simulations. However, it has to be pointed out that our data were not available at the time the modelling studies were performed. The models were based on earlier mineralogical observations from some fractures where ettringite precipitation was interpreted to occur before C-S-H (Milodowski et al., 1998). However, we would like to point out that in the course of this project, the investigation of further fracture samples provided clear evidence that C-A-S-H generally precipitates before ettringite.

Another discrepancy is that the models predict that ettringite is the main phase responsible for the clogging of pores within the biomicrite, and not C-A-S-H, as is observed in the natural system. Our study found no evidence of elevated concentrations of S and Al in EDS element maps of the pores of the wallrock adjacent to fractures, which would indicate porosity reduction by the precipitation of ettringite. However, as indicated in Fig. 2, C-A-S-H precipitation at the fracture–rock interface is responsible for reduction in porosity (see also exemplar samples 87–1 and 89–10 in Martin and Leemann (under review)). An example of fracture armouring and porosity reduction by C-A-S-H mineralisation, as modelled by Watson et al. (2016), is shown in Fig. 5.

The modelling studies predict the dissolution of various phases of the host rock to be responsible for the supply of ions required for the precipitation of hydrated cement minerals such as e.g. C-A-S-H or ettringite (e.g. illite present in sample DD-M99-1, Table 2), which is in agreement with the models from Shao et al. (2013) and Soler (2016). However, whether chalcedony, kaolinite, albite and

dolomite (Soler, 2016) are dissolved could not be approved by our observations.

Comparison of the mineral precipitates predicted from the models with the natural system observations in this study reveals some discrepancies. Whereas most models (except Soler (2016) and Watson et al. (2016)) predict the formation of C-S-H (no incorporation of Al), all our analyses also indicated the presence of significant Al within this component of the alteration. Therefore we refer to this phase as C-A-S-H. Shao et al. (2013) invokes the initial formation of zeolites to account for Al released by the dissolution of kaolinite and illite. Although this is potentially feasible, any early zeolite formation is likely to have been overprinted by later mineralisation events at Maqarin, and could not be confirmed by this study. The presence of zeolites at the outer rim of the alkaline alteration zone, as predicted by Shao et al. (2013), Soler (2016) and Watson et al. (2016), may also be possible, but due to analytical limitations, small zeolites precipitates could not be found. However, our study did reveal the formation of Si-Al-rich gels which could result from the carbonation of C-A-S-H in several samples. The formation of katoite or straelingite predicted by Shao et al. (2013) could not be confirmed in the Maqarin mineralisation.

Another issue is the complete dissolution of ettringite resulting from the upstream movement of the reaction front (Watson et al., 2016). However, the presence of ettringite in various samples throughout the flow path contradicts this prediction. Watson et al. (2016) also predicted the formation of thaumasite in the absence of ettringite. However, in all cases thaumasite occurred in combination with ettringite, either as a solid-solution phase or as Al-end member ettringite and thaumasite (Table 2). Ettringite–thaumasite solid solutions were considered in the study by Soler (2016), who employed elevated sulphate and decreased Al concentrations in the fluid. Watson et al. (2016) explain the formation of thaumasite as the result of the sulphate supplied by the dissolution of ettringite and Si supplied by chalcedony dissolution. However, as indicated in section 4.2, single thaumasite patches were only observed after C-A-S-H had already precipitated, thereby providing the source for Si.

The extent of the alteration zones varies between the different studies. The example fracture sample that Steefel and Lichtner (1998) referred to contains a brownish alteration zone up to 22 mm, and we observed a maximum depth of the alteration zone of from 0.3 to < 25 mm. Steefel and Lichtner (1998) as well as Shao et al. (2013) show the presence of secondary precipitates up to 10 mm into the host rock, Soler (2016) up to ~17 mm and Watson et al. (2016) up to ~30 mm. These alteration depths are broadly consistent with our observations (Table 2). However, sample 87–1 which shows the clearest effect of a fracture-armouring case (see section 4.4) has an alteration zone which extends to only 4 mm. Nevertheless, the porosity evolution profiles, as illustrated by sample 87–1 (Fig. 5), have been qualitatively reproduced by all the model studies.

With regard to future modelling studies, we suggest that the models should consider the precipitation of C-A-S-H before ettringite, and account for Al to be incorporated within C-A-S-H, with this phase, rather than ettringite, being responsible as the major porosity reducing phase. Sample 87–10 provides a good exemplar reference sample for comparing the evolution of porosity reduction in model systems.

5. Conclusions

Our observations suggest that water infiltrating along faults led to the hydration of the natural clinker (pyrometamorphic marble) bodies. In the earliest stage, portlandite is presumed to have precipitated initially from the hyperalkaline fluids circulating

through the fractures, and was quickly altered to calcium carbonate as the pH dropped. In the next step C-A-S-H precipitated in the veins and the adjacent biomicrite was infiltrated by the hyperalkaline groundwater, resulting in a reduction of its porosity as C-A-S-H was precipitated in the matrix porosity. This is most pronounced in sample 87–1, where a 1.2 cm thick vein contains an alteration zone in the adjacent biomicrite with matrix alteration penetrating for up to 3–4 mm, accompanied by a significantly reduced porosity. However, infiltration of the biomicrite was not observed in all samples, which is possibly related to the fact that the micropores in the biomicrite were probably already saturated with background groundwater, inhibiting infiltration by hyperalkaline groundwater from the fractures. In this case, transport of hyperalkaline fluid into the host rock matrix was probably governed by diffusion and/or limited advection.

As fluid compositions in the fractures evolved through precipitation of C-A-S-H along the flow path, the sulphate concentration increased and sulphate phases started to precipitate crosscutting C-A-S-H veins, or intruding into the centre of C-A-S-H veins, which dilated as a result of fracture reactivation. The increased sulphate concentration resulted in fillings of ettringite and/or ettringite–thaumasite solid solution. These abundant observations indicate that C-A-S-H precipitated before the sulphate phases reached saturation in the fluid. In the next stage, zeolites were precipitated, presumably in response to a pH decrease, as observed in the distal region of the hyperalkaline plume.

The petrological evidence indicates that all samples are exposed to carbonation by CO₂ uptake. Well-crystallised ettringite, thaumasite and even some of the crystalline C-A-S-H minerals are not sensitive to carbonation, whereas amorphous C-A-S-H gels are. The effect of carbonation resulted in the decomposition of the C-A-S-H gels and the formation of a mixture of Si-Al-rich gel and calcite.

Comparison of our observations with the results from the reactive transport modelling studies reveals two major discrepancies. Firstly, ettringite is precipitated before C-A-S-H in the models, which is related to the fact that our data, showing the reverse sequence of precipitation, were not available at the time these studies were performed. Secondly, according to the models, ettringite is predicted to be the principal phase responsible for the clogging of the pores, whereas our results clearly indicate that C-A-S-H is responsible for the porosity reduction. The porosity reduction is best exemplified in sample 87–1, where C-A-S-H but not ettringite fills the pores of the host rock adjacent to the fracture, resulting in an armoured fracture (Fig. 5). The hydrate phases predicted by the modelling studies (within the scope of the available thermodynamic data) correspond mostly to those we observed. However, the predicted complete dissolution of ettringite due to an upstream movement of the reaction front (Watson et al., 2016) contradicts our findings. Nevertheless, the general porosity evolution profiles determined in all models at the fracture–rock interface qualitatively correspond to our observations made in sample 87–1.

With regard to future modelling studies, we suggest that it would be worthwhile to attempt to precipitate C-A-S-H before ettringite, accounting for C-A-S-H as the porosity reducing agent, referring to our findings in sample 87–1 as a reference case.

Acknowledgements

We thank Nagra and the partners of the LCS project (JAEA, Posiva, RWM and SKB) for financing this project. Furthermore, we thank M. Mazurek (University of Bern) and AE Milodowski (British Geological Survey) for kindly providing the samples, B. Lothenbach (Empa), P. Lura (Empa), C. Walker (JAEA), and D. Savage (Savage Earth) and the other researcher involved in that project for intense

discussion and suggestions. In addition, we would like to thank J. Kaufmann (Empa) for the mercury intrusion measurements, F. Winnefeld (Empa) for measuring the gas diffusivity and B. Ingold (Empa) for the sample preparation. Further we would like to thank the editor Prof. M. Kersten and D. Kulik (PSI) for their constructive reviews. AE Milodowski publishes with permission of the Executive Director of the British Geological Survey (NERC).

Appendix A. Supplementary data

Supplementary data related to this article can be found at <http://dx.doi.org/10.1016/j.apgeochem.2016.05.009>.

References

- Alexander, W.R. (Ed.), 1992. A Natural Analogue Study of the Maqarin, Hyperalkaline Groundwaters. Source Term Description and Thermodynamic Database Testing. Nagra, Wettingen, Switzerland. NAGRA Tech. Rep. (NTB 91–10).
- Barnett, S.J., Macphee, D.E., Lachowski, E.E., Crammond, N.J., 2002. XRD, EDX and IR analysis of solid solutions between thaumasite and ettringite. *Cem. Concr. Res.* 32, 719–730.
- Barrer, R.M., 1977. Cation exchange equilibria in zeolites and feldspaths. In: Sand, L.B., Mumpton, E.A. (Eds.), *Natural Zeolite Occurrences, Properties, Use*, pp. 385–395.
- Bary, B., Sellier, A., 2004. Coupled-carbon dioxide-calcium transfer model for carbonation of concrete. *Cem. Concr. Res.* 34, 1859–1872.
- Clark, I.D., Fritz, P., Seidlitz, H.K., Trimborn, P., Milodowski, A.E., Pearce, J., Khoury, H.N., 1993. Recarbonation of metamorphosed marls in Jordan. *Appl. Geochem.* 8, 473–481.
- Degnan, P.J., Salameh, E., Khoury, H., Milodowski, A.E., Mäder, U.K., White, M., 2013. Tectonic setting, geology and hydrogeology of Maqarin. In: Pitty, A., Alexander, R. (Eds.), *A Natural Analogue Study of Cement Buffered, Hyperalkaline Groundwaters and Their Interaction with a Repository Host Rock IV: an Examination of the Khushaym Matruk (Central Jordan) and Maqarin (Northern Jordan) Sites*. NDA, Moor Row, UK, pp. 21–55. NDA Technical Report.
- Folk, R.L., 1959. Practical petrographic classification of limestones. *Bull. Am. Assoc. Pet. Geol.* 43, 1–38.
- Groves, G.W., Borough, A., Richardson, I.G., Dobson, C.M., 1991. Progressive changes in the structure of hardened C3S cement paste due to carbonation. *J. Amer. Ceram. Soc.* 74, 2891–2896.
- http://www.nagra.ch/g3.cms/s_page/80740/s_name/geolti. (2013). (Geologische Tiefenlager. NAGRA).
- Kaufmann, J., 2010. Pore space analysis of cement-based materials by combined nitrogen sorption – wood's metal impregnation and multi-cycle mercury intrusion. *Cem. Concr. Compos.* 32, 514–522.
- Kaufmann, J., Loser, R., Leemann, A., 2009. Analysis of cement-bonded materials by multi-cycle mercury intrusion and nitrogen sorption. *J. Colloid Interface Sci.* 336, 730–737.
- Khoury, H., Mazurek, M., Alexander, W.R., 1998. In: Smellie, J.A.T. (Ed.), *Geology and Hydrogeology of the Maqarin Area*, vols. I and II. SKB, Stockholm, Sweden. SKB Technical Report, TR-98–04.
- Leemann, A., Loser, R., 2011. Analysis of concrete in a vertical ventilation shaft exposed to sulfate-containing groundwater for 45 years. *Cem. Concr. Compos.* 99, 74–83.
- Leemann, A., Nygaard, P., Kaufmann, J., Loser, R., 2015. Relation between carbonation resistance, mix design and exposure of mortar and concrete. *Cem. Concr. Compos.* 62, 33–43.
- Linklater, C.M. (Ed.), 1998. A Natural Analogue Study of Analogue Cement Buffered, Hyperalkaline Groundwaters and Their Interaction with a Repository Host Rock: Phase II. UK Nirex, Harwell, U.K. Nirex Science Report, S-98–003.
- Martin, L.H.J., Leemann, A., 2014. Maqarin (Jordan) – a Natural Cement Analog Study: Phase Characterization of Four Selected Samples. Empa, Dübendorf. Published in Nagra NAB report 13–090.
- Martin, L.H.J., Leemann, A. A Natural Analog Study to Understand the Long-term Behavior of Cements: Maqarin (Jordan). Empa, Dübendorf, to be published in Nagra NAB report 15–04, submitted for publication.
- Milodowski, A.E., 1994a. Introduction to the Jordan natural analogue project. In: Milodowski, A.E. (Ed.), *Nagra – Interner Bericht 94-74: a Natural Analogue Study of the Maqarin Hyperalkaline Groundwaters: a Draft Report on Hyperalkaline Groundwater/Rock Interaction*. Nagra, Wettingen, Switzerland, pp. 1–7.
- Milodowski, A.E., Hyslop, E.K., Khoury, H.N., Salameh, E., 1994b. Site description and field sampling programme. In: Milodowski, A.E. (Ed.), *Nagra - Interner Bericht 94-74: a Natural Analogue Study of the Maqarin Hyperalkaline Groundwaters: a Draft Report on Hyperalkaline Groundwater/Rock Interaction*. Nagra, Wettingen, Switzerland, pp. 8–48.
- Milodowski, A.E., Cave, M.R., Reeder, S., Smith, B., Chenery, S.R.N., Cook, J.M., 1994c. Aqueous geochemistry at Maqarin. In: Milodowski, A.E. (Ed.), *Nagra - Interner Bericht 94-74: a Natural Analogue Study of the Maqarin Hyperalkaline Groundwaters: a Draft Report on Hyperalkaline Groundwater/Rock Interaction*. Nagra, Wettingen, Switzerland, pp. 49–65.

- Milodowski, A.E., Pearce, J.M., Hyslop, E.K., Hughes, C.R., Inglethorpe, S.D.J., Strong, G.E., Wheal, N., McKenzie, A.B., Karnland, O., Khoury, H.N., 1994d. Mineralogy and petrology. In: Milodowski, A.E. (Ed.), Nagra - Interner Bericht 94-74: a Natural Analogue Study of the Maqarin Hyperalkaline Groundwaters: a Draft Report on Hyperalkaline Groundwater/Rock Interaction. Nagra, Wettlingen, Switzerland, pp. 66–141.
- Milodowski, A.E., Hyslop, E.K., Pearce, J.M., Wetton, P.D., Kemp, S.J., Longworth, G., Hodginson, E., Hughes, C.R., 1998. Mineralogy, petrology and geochemistry. In: Smellie, J.A.T. (Ed.), Maqarin Natural Analogue Study: Phase III, vols. I and II. SKB, Stockholm, Sweden, pp. 135–180. SKB Technical Report, TR-98-04.
- Milodowski, A.E., Trotignon, L., Khoury, H., Salameh, E., Arnal, N., Bienvenu, P., Bulle, C., Chenery, S.R., Crouzet, N., Fontanini, L., Hodginson, E.S., Mäder, U., McKervey, J., Peycelon, H., Pontremol, S., Rassineux, F., Raynal, J., Rose, J., Vandamme, D., 2013. The analogue cement zone (ACZ). In: Pitty, A., Alexander, R. (Eds.), A Natural Analogue Study of Cement Buffered, Hyperalkaline Groundwaters and Their Interaction with a Repository Host Rock IV: an Examination of the Khushaym Matruk (Central Jordan) and Maqarin (Northern Jordan) Sites. NDA, Moor Row, UK, pp. 97–226. NDA Technical Report.
- Münch, B., Martin, L.H.J., Leemann, A., 2015. Segmentation of elemental EDS maps by means of multiple clustering combined with phase identification. *J. Microsc.* 260, 411–426.
- Pettijohn, F.J., 1975. *Sedimentary Rocks*, third ed. Harper and Row, New York.
- Pitty, A., Alexander, R. (Eds.), 2014. A Natural Analogue Study of Cement Buffered, Hyperalkaline Groundwaters and Their Interaction with a Repository Host Rock IV: an Examination of the Khushaym Matruk (Central Jordan) and Maqarin (Northern Jordan) Sites. NDA, Moor Row, UK. NDA Technical Report.
- Savage, D., 1998. In: Smellie, J.A.T. (Ed.), Zeolite Occurrence, Stability and Behaviour, vols. I and II. SKB, Stockholm, Sweden, pp. 281–303. SKB Technical Report, TR-98-04.
- Savage, D., 2011. A review of analogues of alkaline alteration with regard to long-term barrier performance. *Min. Mag.* 75, 2401–2418.
- Schmidt, T., Lothenbach, B., Romer, M., Scrivener, K., Rentsch, D., Figi, R., 2008. A thermodynamic and experimental study of the conditions of thaumasite formation. *Cem. Concr. Res.* 28, 337–349.
- Shao, H., Kosakowski, G., Berner, U., Kulik, D.A., Mäder, U., Kolditz, O., 2013. Reactive transport modeling of the clogging process at Maqarin natural analog site. *Phys. Chem. Earth* 64, 21–31.
- Smellie, J.A.T., 1998. In: Smellie, J.A.T. (Ed.), Maqarin Natural Analogue Study: Phase III, vols. I and II. SKB, Stockholm, Sweden. SKB Technical Report, TR-98-04.
- Smellie, J.A.T., Salameh, E., Clark, I.D., Milodowski, A.E., 2013. Hydrogeochemistry. In: Pitty, A., Alexander, R. (Eds.), A Natural Analogue Study of Cement Buffered, Hyperalkaline Groundwaters and Their Interaction with a Repository Host Rock IV: an Examination of the Khushaym Matruk (Central Jordan) and Maqarin (Northern Jordan) Sites. NDA, Moor Row, UK, pp. 55–96. NDA Technical Report.
- Soler, J.M., 2016. Two-dimensional reactive transport modeling of the alteration of a fractured limestone by hyperalkaline solutions at Maqarin (Jordan). *Appl. Geoch.* 66, 162–173.
- Steeffel, C.I., Lichtner, P.C., 1998. Multicomponent reactive transport in discrete fractures II: infiltration of hyperalkaline groundwater at Maqarin, Jordan, a natural analog site. *J. Hydrol.* 209, 200–224.
- Thomas, M.D.A., Matthews, J.D., Haynes, C.A., 1992. Carbonation of fly ash concrete. *ACI Spec. Publ.* 19, 539–556.
- Waber, H.N., Clark, I.D., Salameh, E., Savage, D., 1998. Hydrogeochemistry of the Maqarin area. In: Smellie, J.A.T. (Ed.), Maqarin Analogue Study: Phase III, pp. 181–235. SKB Technical report TR-98-04.
- Watson, C., Wilson, J., Savage, D., Benbow, S., Norris, S., 2016. Modelling reactions between alkaline fluids and fractured rock: the Maqarin natural analogue. *Appl. Clay Sci.* 121–122, 46–56.
- Weber, H., 1983. *Steinkonservierung*. Expert-Verlag, Grafenau, Deutschland.
- Wierig, H.J., 1984. Longtime studies on the carbonation of concrete under normal outdoor exposure. In: Proc. RILEM Seminar on the Durability of Concrete Structures under Normal Outdoor Exposure, pp. 239–249.